Simulations for Developing the Fog Sensor NebioSens

Martin Löffler-Mang, Dominik Schön
University of Applied Sciences
Saarbrücken, Germany
loeffler-mang@htw-saarland.de

Christian Ruckstuhl
inNET Monitoring AG
Altdorf, Switzerland
christian.ruckstuhl@innetag.ch

Abstract - ***In this paper mainly simulations for developing the fog sensor NebioSens are presented. After some basic principles of light barriers, alternating beam technology, and fog the first ideas of a mechanical construction for sensor housing are shown. Then some single particle simulations with Mie scattering open the simulation results. Furthermore, ensemble simulations for typically 100 million light rays within the measuring area are calculated with ZEMAX, a ray tracing software tool. Finally, first visibility estimation will be outlined.***

Keywords—fog sensor; optical sensor; drops simulation; visibility; ZEMAX *(key words)*

I. INTRODUCTION

Observations during the 20th century (summarized by Pruppacher and Klett [1]) show that fog, unlike clouds, is characterized by small particles (typically between 2.5 μm and a few tens of micrometers, with a typical mean diameter between 10 and 20 μm), small number concentrations (one to a few hundreds per cubic centimeter), and liquid water contents ranging from 0.05 to 0.5 g/m^3.

Atmospheric turbidity is caused by aerosols and hydrometeors. The types and concentrations of these particles also are responsible for visibility (Heintzenberg et al. [2], Beard [3]). Common method to estimate visibility was the observation of targets in the near or far neighborhood with known distance. But all over the world automatic sensors are under development to replace observers.

In order to measure visibility with optical instruments two physical effects are important. On the one hand there is scattering when light is sent into a measuring volume, and on the other hand there is absorption. Both effects are working when using a transmissometer and measuring the fraction of emitted light, that is reaching the detector. Transmissometers are large and expensive; they need a measuring volume of at least several meters in length.

In systems, that use only scattered light, the detector is placed under a certain angle to the light source. The measured quantity is the portion of light scattered into the chosen direction by the particles in the measuring volume. The intensity of scattered light does not only depend on the angle, but also on the type of particles. Therefore, a classical device from the lab using scattered light does not deliver clear results as long as the type of particles is unknown (e.g. drops, dust, ice crystals).

The idea of the sensor development presented in this paper is based on own preparatory work (Löffler-Mang [4], Steffen [5]) and contains a system with a number of detectors around the measuring volume. The aim is to develop an inexpensive and easy to use prototype sensor for fog and cloud particles. On the one hand the scattering properties of different particles under certain angles will be used to discriminate between liquid and ice particles. On the other hand, the intensity of scattered light and the extinction in forward direction will be used to estimate visibility.

II. BASIC OF PRINCIPLES

A. Light Barriers

All lights barriers consist of a light source as transmitter – preferably LEDs and laser diodes – and a receiver, mostly a photo diode. There are three basic types of construction: (a) the transmission light barrier, (b) the reflection light barrier, and (c) the off-axis light barrier, see figure 1. The figures and the equations in this section are taken from Löffler-Mang [6].

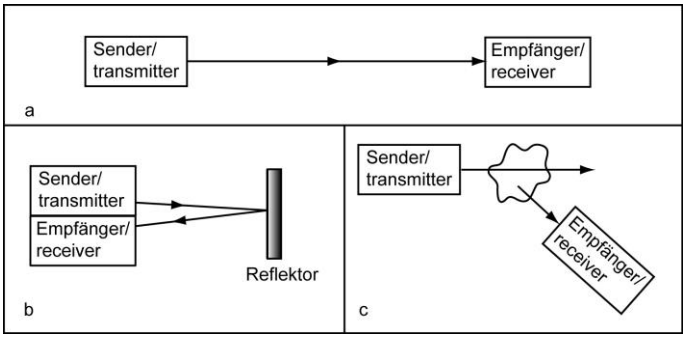

Figure 1: Principal set-ups of light barriers,
(a) transmission, (b) reflection, (c) off-axis

The measurement principle of type (a) and (b) is the same: due to a partial or total interruption of the light beam the output voltage of the receiver will change. Type (c) works only, if particles in the light beam scatter the light into the direction of the receiver.

A great number of applications is based on these three types: alarm systems, passive infrared detector alarm systems, light barriers for dangerous machines, height monitoring in tunnels, fork light barriers for measuring the number of rotations, smoke detectors, turbidity measurement, and some more special techniques. In this paper the simulations for developing the fog sensor NebioSens are explained in more detail.

B. Measurement of Turbidity

To evaluate the quality of water the turbidimetry is used besides other techniques. The light beam passes through a small test-tube, which is filled with the water under investigation. The light extinction and the light scattering under an angle of 90° are measured, see figure 2.

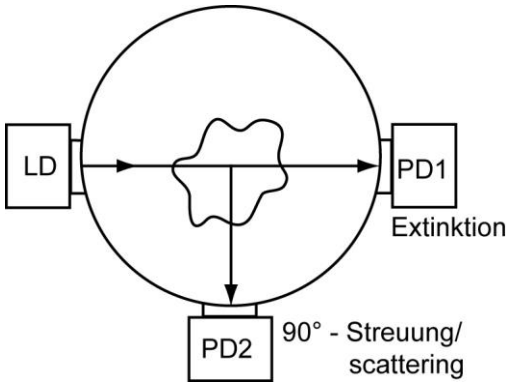

Figure 2: Set-up for the measurement of turbidity with one laser diode (LD) and two photo diodes (PD1 for extinction, PD2 for scattering at 90°)

The problem with this measurement method could be dirt on the windows and variations in the light intensity, which would distort the signals. To eliminate distortion an alternating four-beam-technique was evaluated (Bochter [7]). Two alternating beam sources LDA and LDB send their light into the medium under investigation and the two receivers PD1 and PD2 measure the intensities I1A and I2A resp. I1B and I2B, see figure 3.

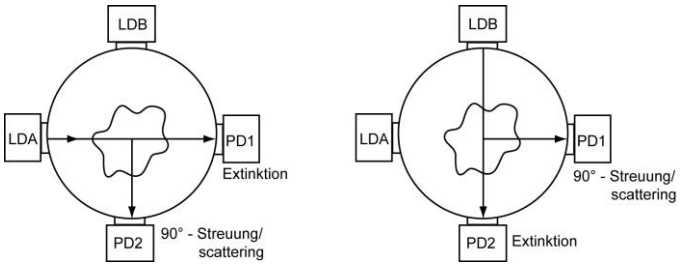

Figure 3: Alternating four-beam-technique with two transmitters (LDA and LDB) as well as two receivers (PD1 and PD2)

The signal on PD1 with a beam from LDA is given to

$$I_{1A} = I_A \varepsilon f_1 \tag{1}$$

with the intensity I_A of the transmitter, the extinction coefficient ε and the window damping f_1. For PD2 we have:

$$I_{2A} = I_A \varepsilon \sigma f_2 \tag{2}$$

with σ as additional scattering coefficient. Two similar equations are formed when the beam comes from LDB. Hence we have:

$$\frac{I_{1A}}{I_{2A}} = \frac{I_A \varepsilon f_1}{I_A \varepsilon \sigma f_2} = \frac{1}{\sigma}\frac{f_1}{f_2} \tag{3}$$

$$\frac{I_{1B}}{I_{2B}} = \sigma \frac{f_1}{f_2} \tag{4}$$

This step leads to the elimination of the transmitter intensities and the extinction coefficient. In a second step we eliminate the damping relation f_1/f_2:

$$\sigma \frac{I_{1A}}{I_{2A}} = \frac{1}{\sigma}\frac{I_{1B}}{I_{2B}} \tag{5}$$

Thus we get the scattering coefficient σ without any disturbances:

$$\sigma = \sqrt{\frac{I_{1B} I_{2A}}{I_{1A} I_{2B}}} \tag{6}$$

C. Fog Sensor

Transmissometers are used to measure the visibility range in a foggy environment. These systems contain light barriers with typical distances of 50 m or 300 m between transmitter and receiver. Such systems are installed in Germany, e.g. along the motorway A8 between Stuttgart and Ulm.

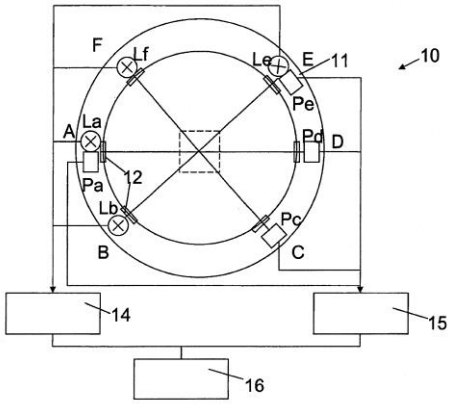

Figure 4: Patented set-up of a fog sensor with four transmitters (La, Lb, Le, and Lf) as well as four receivers (Pa, Pc, Pd, and Pe), details and explanation of the numbers can be found in the European patent PCT/EP2007/006183 [8]

A new data evaluation enables to distinguish the different fog types into drop fog, ice fog, and mist. The different scattering characteristics of the particles depending on the scattering angle are used. Several receivers surround a measurement area to measure both the forward and the backward scattering under determined angles. Figure 4 shows the schematic set up of a fog sensor.

It is possible to extend the alternating four-beam-technique from the turbidity measurements to several beams and to apply it to NebioSens. Then the results of the fog sensor will no longer depend on dirty or dusty windows nor on variations of the light intensity of the transmitter (Löffler-Mang and Steffen [8]).

III. MECHANICAL CONSTRUCTION

First experiments started with some light sources and detectors mounted in a ring element having a diameter of approx. 20 cm. In figure 5 this ring can be seen in addition with a small ultrasonic nozzle to prepare fog consisting of drops.

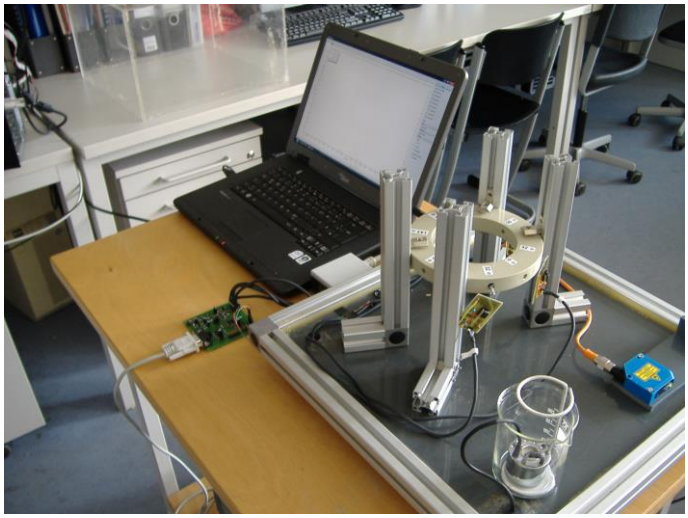

Figure 5: First experimental set-up for producing fog and measuring the scattered light with detectors mounted in ring element.

Based on this first experiments a mechanical housing was constructed, which is shown in figure 6. Again the ring element can be seen with holes for one laser diode and three photo diodes. In addition, there is space for the necessary electronics. And of course there will be a cover on top of the housing with just a circular opening at the inner ring. This 3D-model of the mechanical construction was also used for the optical ensemble simulations presented in a later chapter.

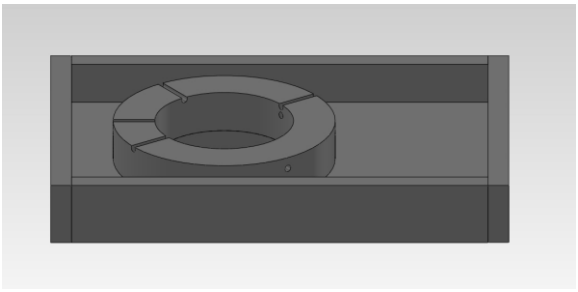

Figure 6: Simulated mechanical construction.

IV. SINGLE PARTICLE SIMULATIONS

To start with the simulations single particles were chosen. Only spherical particles were selected, therefore, an open source Mie scattering software could be used (Bohren and Huffman [9]). Figure 7 shows the scatter diagram for water drops with 10 µm (blue line) and 20 µm (red line) in diameter. A relative intensity is shown as a function of scattering angle. The typical behavior can be seen with a strong maximum in direct forward scattering and with a large number of side lobes, for larger drops being narrower than for smaller drops. The minimum intensity is found at an angle of approx 90 to 100 degrees.

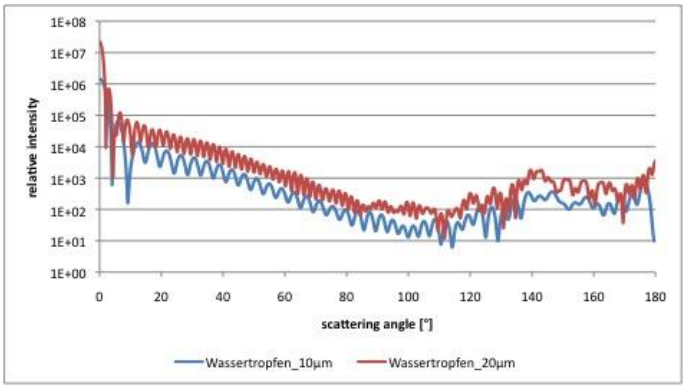

Figure 7: Mie scattering for single smaller (blue line) and larger (red line) water drops, relative intensity as a function of scattering angle.

In the next step, figure 8 shows the comparison between a water drop (blue line) and a spherical sand particle (green line), both having a diameter of 20 µm. The only difference in the simulations is the index of refraction. For H_2O a value of n=1,33 was used, for SiO_2 a value of n=1,52. In forward scattering direction the curves look similar but there appears a significant difference in backward scattering direction between 130 and 160 degrees. This difference will give the possibility to discriminate between particle types, as it will be explained later on.

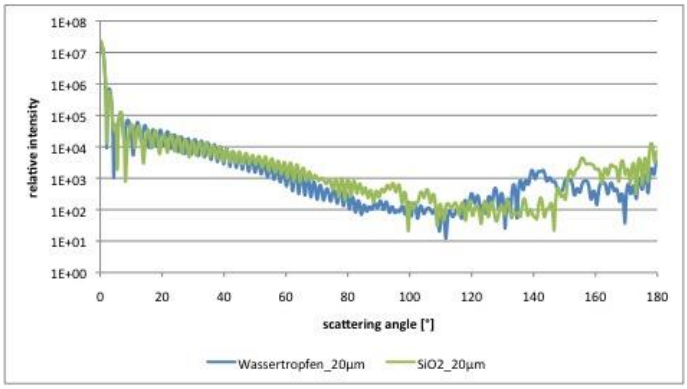

Figure 8: Mie scattering for single water drop (blue line) and sand particle (green line), relative intensity as a function of scattering angle.

Standard photo detectors do not collect the scattered light with an angular resolution as shown in figure 8. They typically have an aperture angle of approx. 20 degrees. To simulate this behavior in figure 9 the results shown before are averaged in 20-degree steps. Again the curves look similar in forward scattering direction and show a significant difference around 140 degrees in backward scattering direction.

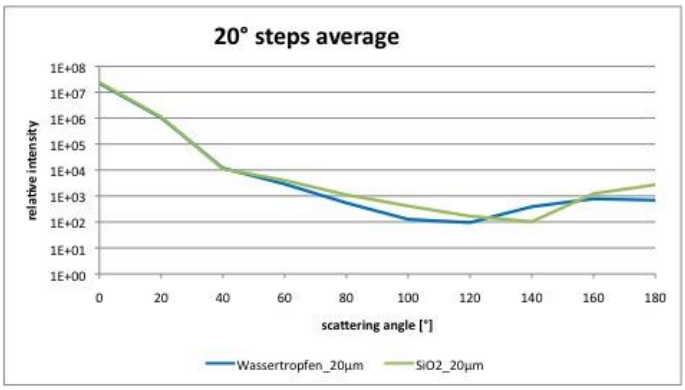

Figure 9: Mie scattering for single water drop (blue line) and sand particle (green line), relative intensity as a function of scattering angle, average values for 20-degree steps.

In the next step we want to discriminate between particle types. Therefore, the values for relative intensities at approx. 40 (forward) and 140 (backward) degrees are taken from the data and the ratio of forward to backward scattered intensity is calculated. This was done for water drops and sand particles with a diameter of 20 µm as shown in figure 9 but also for water and sand with diameter of 10 µm. The resulting ratios are shown in table 1.

Table 1: Ratios for forward (40°) to backward (140°) scattered intensities, water drops and spherical sand particles with 10 and 20 µm.

	10 µm	20 µm
water drop	17	16
spherical sand particle	11	11

The water drops show ratios of 17 (for 10 µm diameter) and 16 (20 µm), whereas the spherical sand particles for both sizes show a ratio of 11. This means e.g. for sand, that the intensity of light scattered in forward direction (40° +- 10°) is by a factor of 11 higher than the one scattered backward (140° +- 10°). Furthermore, we can see, that there is nearly no influence of particle size on the ratios. But there exists a significant difference in the ratios between water drops and sand particles. Due to this finding the ratio of forward to backward scattered light can be used to discriminate between particle types. From earlier experiments we know, that this is even valid for particle ensembles and for other types of particles e.g. ice and dust particles in agreement with Macke et al. [10], Mishchenko et al. [11], and Macke [12].

V. ENSEMBLE SIMULATIONS

Let us come back to ensembles of particles with physical values as mentioned in the introduction. In this chapter simulation results are presented for monodispers water and sand particles within the mechanical set-up shown in figure 6. Simulations were done with 100 million rays per case; particle concentration was varied between 50, 500, 1000, and 2000 cm^{-3}, particle diameter between 10, 20, and 40 µm. Only selected cases will be shown and for all figures one out of 1000 rays is drawn.

In figure 10 the detector signal is shown in 0° forward direction without particles in the measuring volume. The colors give the number of beams on the square detector array with an area of 1mm by 1mm. Approx. 91.1 million rays hit this detector array, representing a total optical power of 4.56 mW. This is the reference value for all further simulations.

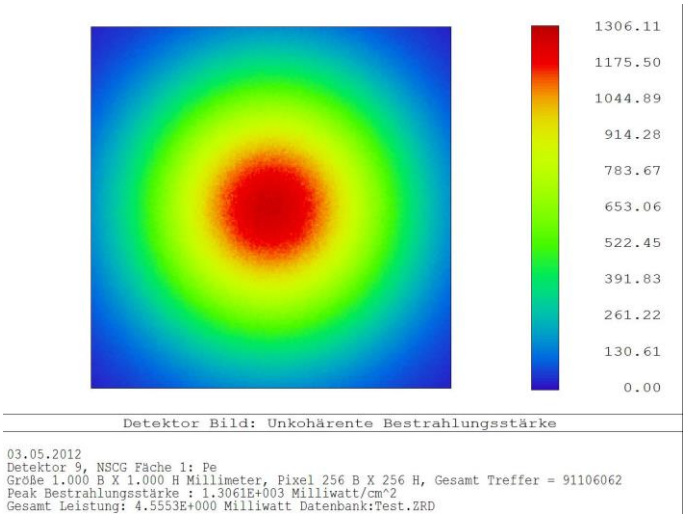

Figure 10: Total power on detector in 0° forward direction of 4.56 mW, reference simulation without particles.

The first simulation results are shown in figure 11 for water drops inside the measuring volume with drop diameter of 10

µm and a number concentration of 1000 cm^{-3}. The light is entering the measuring volume from the lower left side; the detector positions can be seen on the sensor ring element. Obviously most rays pass through the water drops without any interaction. Only a few rays are scattered and the direction is mainly forward. This is of course in qualitative correspondence with the Mie scattering from a single drop shown in figure 7.

As mentioned above, 10 thousand out of 100 million rays are shown in figure 11 to keep the figure clear. In the figure no ray hits the backward oriented detector. This is not true when taking all rays into account, but the number is still too low for a quantitative analysis.

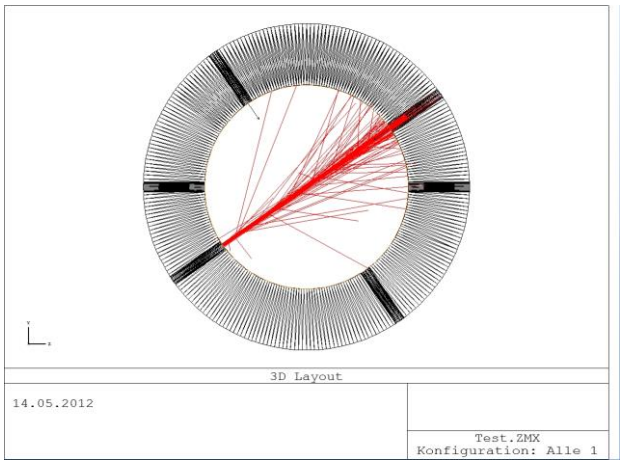

Figure 11: Ensemble simulation for water drops; drop diameter 10 µm, number concentration 1000 cm^{-3}.

Further results are shown in figure 12 for larger water drops with a diameter of 20 µm and the same number concentration of 1000 cm^{-3}. The situation is similar as in the first simulation, but the scattering of the larger drops is much stronger as expected.

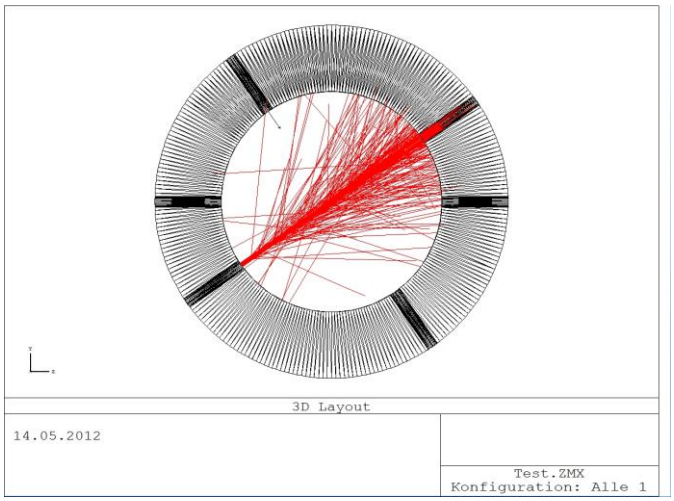

Figure 12: Ensemble simulation for water drops; drop diameter 20 µm, number concentration 1000 cm^{-3}.

Other results are shown in figure 13 for larger sand particles with also a size of 20 µm as a 3D-plot. The qualitative view shows a slightly rougher scattering in comparison to the large water drops. Therefore, the ratio of forward to backward scattered light should decrease a little bit in agreement with the single particle simulations.

As a last result some simple estimation for visibility according to particle number concentration is given. We assume an exponential decrease of light intensity with the path length in a fog:

$$P(x) = P_0 e^{-\sigma_e x} \tag{7}$$

with P_0 being the intensity at the beginning and P(x) the intensity after the path length x; σ_e is the extinction coefficient of the fog in the measuring volume.

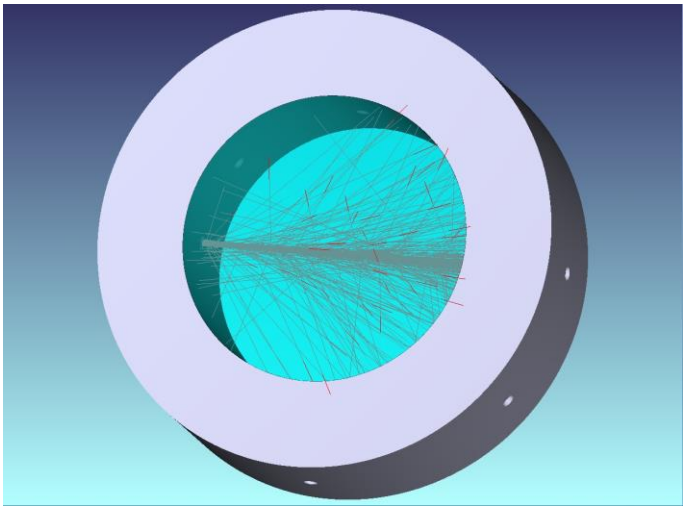

Figure 13: Ensemble simulation for sand particles; particle size 20 µm, number concentration 1000 cm^{-3}.

Furthermore, we need a relation between extinction coefficient and visibility. For this purpose we take the often-used relation:

$$Vis = \frac{-\ln(0.05)}{\sigma_e} = \frac{3}{\sigma_e} \tag{8}$$

Herein the assumption is used, that a contrast of at least 5 % is needed to discriminate between objects in fog.

From the ensemble simulations we know the intensity on the detector in 0° forward direction for each case. Furthermore, we know the transmitted intensity, see figure 10. With the dimensions of the mechanical construction the extinction coefficient can be calculated for each number concentration according to equation 7. In the last step the visibility can be estimated from equation 8. These visibilities are summarized in table 2.

Table 2: Visibility as a function of drop number concentration for monodispers water drops with 20 μm in diameter.

drop number concentration [cm^{-3}]	50	500	1000	2000
visibility [m]	148.3	12.0	5.9	2.4

Obviously the number concentrations chosen for the simulations are quite high, the visibility is rather low due to the very dense fog conditions. We had had the aim to evaluate the simulations also quantitatively; therefore we had used the high number concentrations. But we learned, that simulations with even more than 100 million rays have to be done in the future

VI. Conclusion And outlook

In this paper simulations to develop a fog sensor were presented. It could be shown from single particle simulations, that discrimination between fog particle types is possible by using the ratio of forward to backward scattered light. This ratio is approx. 17 for water drops and only approx. 11 for sand particles (as model particles for dust). In addition, the ensemble simulations showed a similar qualitative behavior. Finally, from the ensemble simulations the visibility could be estimated using the extinction signal in 0° forward direction.

The next steps on the way towards the aim of developing a inexpensive and easy to use prototype sensor are explained in this last section. An older version of a ring type sensor already exists. Now the new mechanical construction shown in figure 6 will be built up to verify the simulations by experiments. A fog chamber will be used, that also exists from preparatory studies with students. To include also ice particles in the experiments it will be necessary to enlarge the fog chamber and to develop a possibility to produce ice particle fog. In addition, it is intended to use a wind tunnel test facility at Goethe University in Mainz (v. Blohn et al. [13]) for some ice particle experiments.

In the field of simulations also some more work has to be done. The number of rays in the ensemble simulations has to be increased for quantifying the forward to backward scattering intensity ratios. And agreement between simulations and experiments should be reached.

From today's point of view the last step will be the implementation of the alternating beam technology into the prototype sensor. With this integration the sensor will become independent from dust and fog on the windows as well as from intensity variations of the transmitting light sources within NebioSens.

References

[1] H.R. Pruppacher and J.D. Klett, *Microphysics of Clouds and Precipitation*, 2nd ed., Kluwer Academic Publishers, 1997, pp. 10-23.

[2] J. Heintzenberg, M. Wendisch, B. Yuskiewicz, D. Orsini, A. Wiedensohler, F. Stratmann, G. Frank, B.G. Martinsson, D. Schell, S. Fuzzi and G. Orsi, "Characteristics of Haze Mist and Fog," *Contrib. Atmos. Phys.* 71, 1998, pp 21-31.

[3] K.V. Beard, "Terminal Velocity and Shape of Cloud and Precipitation DropsAloft," *J. Atmos. Sci*. 33, 1976, pp 851-864.

[4] M. Löffler-Mang, "A Laser-Optical Device for Measuring Cloud and Drizzle Drop Size Distributions," *Meteorol. Z. N.F.*,7, 1998, pp 53-62.

[5] R. Steffen, "Entwicklung eines optischen Sensorprototyps zur Nebelcharakterisierung und Sichtweitenbestimmung," *Diploma Thesis*, 2005.

[6] M. Löffler-Mang, *Optische Sensorik, Lasertechnik, Experimente, Light Barriers*, Vieweg + Teubner Verlag, Springer Fachmedien, 2012, pp. 156-163.

[7] K. Bochter, "Streulichtphotometer nach dem Vierstrahl-Wechsellicht-Verfahren," *DE 43 34 208 A 1*, German patent, 1995.

[8] M. Löffler-Mang and R. Steffen, "Vorrichtung und Verfahren zur Unterscheidung von Nebelarten," *PCT/EP2007/006183*, European patent, 2007.

[9] C.F. Bohren and D.R. Huffman, "Absorption and Scattering of Light by Small Particles," Wiley and Sons New York, 1983.

[10] A. Macke, J. Mueller and E. Raschke, "Single Scattering Properties of Atmospheric Ice Crystals," *J. Atmos.Sci.*, 53, 1996, pp 2813-2825.

[11] M.I. Mishchenko, L.D. Travis and D.W. Mackowski, "T-matrix computations of light scattering by nonspherical particles: a review," *J. Quant. Spectrosc. Radiat. Transfer*, 55, 1996, pp 535-575.

[12] A. Macke, "Monte Carlo calculations of light scattering by large particles with multiple internal inclusions. In: M.I. Mishchenko, J.W. Hovenier and L.D. Travis (Hrsg.): *Light Scattering by Nonspherical Particles, 10*," Academic Press, San Diego, 2000, pp 309-322.

[13] N. v. Blohn, K. Diehl, S.K. Mitra and S. Borrmann, "Windtunnel investigations on the growth rates and regimes, and the collection kernels during riming," *J. Atmos.Sci.*, 66, 2009, pp 2359-2366.